

Accelerated Synthesis of Ordered Mesoporous Carbons Using Plasma

Anthony Griffin, Genwei Chen, Mark Robertson, Kun Wang, Yizhi Xiang,* and Zhe Qiang*

Cite This: *ACS Omega* 2023, 8, 15781–15789

Read Online

ACCESS |



Metrics & More

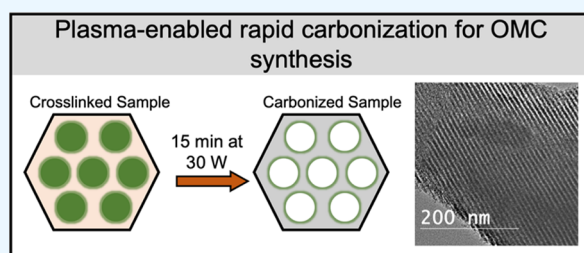


Article Recommendations



Supporting Information

ABSTRACT: Conventional ordered mesoporous carbon (OMC) production usually requires long processing times in the carbonization step to achieve desired temperatures through controlled ramps. To enable expedited materials discovery, developing advanced manufacturing capability with significantly improved throughput is highly desired. Current approaches for accelerating the synthesis of OMCs include using microwave and Joule heating. However, both methods rely on the introduction of additional components, such as microwave absorbers and electrically conductive agents, within the bulk materials to impart the ability to reach high carbonization temperatures. This work demonstrates accelerated synthesis and functionalization of OMCs through the use of a dielectric barrier discharge plasma, where carbonization can be accomplished within 15 min using 30 W plasma sources, representing more than an order of magnitude increase in polymer-to-carbon conversion kinetics compared to that of a traditionally pyrolyzed analogue. Particularly, the ability of performing rapid carbonization without the use of additional substrates within the OMC precursor systems is advantageous. A systematic investigation of how plasma power, time, and gas atmosphere impact the resulting OMC pore textures and properties is performed, demonstrating the broad applicability of plasma-enabled carbonization methods. Furthermore, we demonstrate that the plasma treatment strategy can be extended to incorporate heteroatoms into the carbon framework by introducing ammonia gas, resulting in OMCs with a nitrogen content up to 4.7 at %, as well as non-Pluronic templating systems for synthesizing OMC with pore sizes larger than 10 nm. As employing a plasma source for materials pyrolysis is an industrially relevant approach, our system can be extended toward scaled synthesis of OMCs with much faster production rates.



1. INTRODUCTION

Ordered mesoporous carbons (OMCs) have attracted significant interest due to their advantages of excellent pore accessibility, relatively high surface areas, and uniform pore size distributions.^{1,2} Enabled by these properties, OMCs have great potential in various applications such as air and water purification,^{3–5} gas storage,^{6–8} shape-selective catalysis,^{9–11} biomedicine,^{12–14} and electrochemical energy storage.^{15–19} Conventional OMC synthesis methods involve the use of prefabricated mesoporous templates and/or self-assembled polymer materials.²⁰ Particularly, the soft-templating approach has been widely employed since their inception, which uses amphiphilic surfactants and/or copolymers to direct the nanostructure of carbon precursors (e.g. resol).^{21–23} Upon crosslinking, ordered resol/polymer blends can be pyrolyzed at high temperatures (≥ 600 °C) under an inert atmosphere to produce OMCs. In general, the entire process involves a relatively long processing time.²⁰ Specifically, the pyrolysis step requires a controlled temperature ramp for reaching the desired carbonization temperature, which could take at least several hours for accomplishing a heating–cooling cycle. Looking forward, advances in combinatorial materials discovery for many nanotechnological applications would demand

material synthesis and production with substantially improved throughputs.^{24,25}

For OMC materials, opportunity exists in expediting the carbonization process, reducing the associated time from many hours to minutes.^{26,27} For example, microwave irradiation has been utilized as a viable option for rapid OMC production, where the carbonization of precursors can be achieved within a few minutes.^{28,29} While effective, this method requires the presence of conductive substrates/chemical agents within the polymer system, serving as microwave absorbers, as most polymers have very limited microwave heating ability. Alternatively, ultrafast carbonization through Joule heating has been employed for various polymer precursors.^{30–32} For example, self-assembly with non-equilibrium annealing phase transformation was carried out with amphiphilic block copolymers and carbon precursors.³³ Subsequently, Joule

Received: March 6, 2023

Accepted: April 6, 2023

Published: April 17, 2023



heating was employed to complete the carbonization process, resulting in rapid synthesis of OMCs containing different nanoparticles within 2 min, using a range of different input power from 70 to 420 W. However, this method requires the presence of additional components (i.e., electrically conductive agents) to impart a Joule heating capability to the block copolymer and resol blends.

Using plasma sources for achieving accelerated carbonization is an industrially relevant process, which can enhance reaction kinetics while minimizing materials decomposition observed in traditional carbonization methods.^{34–36} During plasma treatment, the carbon precursor surface interacts with energetic species, such as radicals, ions, hot electrons, and atoms and/or molecules in excited states, consequently, achieving simultaneously fast carbonization and carbon surface functionalization. Plasma treatment has been found to change the surface-energy-dispersive and polar components of carbon model surfaces and carbon fibers.³⁷ As an example, Lee et al. developed a two-step carbonization process using microwave plasma for carbon fiber production,³⁸ employing polyacrylonitrile as a precursor, with an initial hold at 100 W followed by a carbonization step at 1000 W. Similarly, a plasma jet has been utilized for the carbonization of activated carbon from coffee ground waste.³⁹ Using a rotating gliding arc generator with a N₂ plasma jet, activated carbon was produced with controllable pore sizes upon varying the processing conditions. Gallucci et al.⁴⁰ reported a plasma-assisted synthesis of nitrogen-doped (N-doped) carbon dots, where plasma-generated electrons accelerated carbon dot production and promoted initiation of reactant condensation. Furthermore, nitrogen heteroatoms were successfully incorporated in the carbon dots using 5 kV plasma treatment for 2 h. In these examples, the chemical composition and morphology of resulting carbon materials can be controlled by several processing parameters of plasma treatment, including voltage, exposure time, and plasma/gas atmosphere. Moreover, heteroatom-containing gas mixtures may be further utilized during plasma-assisted carbonization to dope the carbon framework, providing additional opportunities for further tailoring OMC material properties and functionality.^{41–43} Specifically, utilization of nitrogen and ammonia gases during plasma treatment has been reported to introduce nitrogen functional groups on carbon fiber surfaces.^{44,45} While plasma-assisted carbonization provides a facile approach in functional carbon production, only microwave plasma, plasma jet, and plasma torch were used. To the best of our knowledge, dielectric barrier discharge (DBD) plasma has not been studied for the carbonization process. The DBD plasma-activated species can further react with the produced OMC, realizing simultaneous surface doping during the carbonization process. However, the use of plasma for such synergized carbonization and surface doping process is still underexplored.

Herein, we demonstrate the use of DBD plasma for accelerating OMC synthesis in which carbonization can be accomplished within 15 min using 30 W plasma sources, representing an order of magnitude faster kinetics compared to conventional approaches that take several hours. The power deposition of the DBD plasma is significantly lower than the microwave plasma and Joule heating methods mentioned above, suggesting that this method could be useful toward decarbonization/electrification of industrial processes. A Pluronic-templated OMC system was selected as a model system for systematic investigations of how plasma power, time, and gas atmosphere impact the resulting OMC pore

texture and properties. These results are also compared with their counterparts prepared using a conventional electric furnace for the carbonization process. The materials decomposition mechanism upon pyrolysis is studied through mass spectrometry (MS), providing fundamental insights about polymer-to-carbon conversion using different carbonization approaches. Furthermore, we show that the simultaneous carbonization and N-doping can also be realized, demonstrating that this process can be extended to non-Pluronic-templated systems, confirming the broad and robust applicability of the plasma-enabled carbonization method for synthesizing functional OMC materials.

2. EXPERIMENTAL SECTION

2.1. Materials. Phenol (>99%), hydrochloric acid (HCl; ACS reagent, 37%), sodium hydroxide (NaOH), potassium hydroxide (KOH), poly(propylene oxide)-*block*-poly(ethylene oxide)-*block*-poly(propylene oxide) triblock copolymer (Pluronic F127; PEO₁₀₆-PPO₇₀-PEO₁₀₆), tetraethyl orthosilicate (TEOS; >98%), and dichloromethane (99.9%) were obtained from Sigma-Aldrich. Formaldehyde (37 wt % in H₂O; contains 10–15% methanol as a stabilizer) was purchased from TCI, and ethanol (190 proof) was obtained from Decon Labs. Poly(styrene)-*block*-poly(2-vinyl pyridine) (PS-*b*-P2VP; M_n : 114,000 Da, 48 vol % PS, polydispersity: 1.05) was purchased from Polymer Source Inc. All chemicals were used as received without further purification. Deionized (DI) water was obtained by passing tap water through a Milli-Q IQ 7003 ultrapure lab water purification system from Millipore Sigma.

2.2. Sample Preparation. Low-molecular-weight phenolic resin (resol) was synthesized by the condensation of phenol and formaldehyde under basic (NaOH) conditions following a previous report.⁴⁶ The preparation of OMC also followed an established protocol.⁴⁷ In brief, 4.8 g of Pluronic F127 was first dissolved in a mixture of 3 g of 0.2 M HCl and 24 g of ethanol. The solution was heated to 42 °C and stirred for 1 h until a homogenous mixture was obtained. A 15 g resol solution (20 wt % in ethanol) and 6.24 g of TEOS were then added to the solution and stirred for 2 h at 42 °C. For non-Pluronic-templated samples, PS-*b*-P2VP was physically mixed with resol to achieve a total of 30 wt % hydrophobic content in the blend system (specifically, 6.25 g of PS-*b*-P2VP and 3.75 g of resol were blended). Subsequently, the solutions were then drop cast into several Petri dishes and dried overnight through solvent evaporation. The films were then crosslinked at 100 °C for 24 h prior to carbonization.

The DBD plasma-assisted carbonization was performed in a coaxial DBD reactor consisting of a quartz tube with an inner diameter of 7 mm and an outer diameter of 3/8". The reactor system has been shown in our previous report, although the specific reactor parameters are different.⁴⁸ Specifically, a 6 cm long stainless steel mesh (20 mesh) was employed as the outer electrode and wrapped tight around the quartz tube. The out electrode was wrapped with ceramic fiber for insulation. A 1/16" tungsten electrode was inserted at the center of the reactor and acted as the inner electrode. The discharge volume of the DBD reactor was 2.2 cm³ without the polymer precursor. The DBD plasma was generated using a PMV500 high-voltage AC power source. The applied voltage was measured using an oscilloscope (Tetronix MDO32 3-BW-100) connected to a high-voltage probe (1000:1, Tektronix P6015A), and the gas voltage was measured across a 10 nF capacitor by the same oscilloscope with a TPP0250 voltage probe. The power input

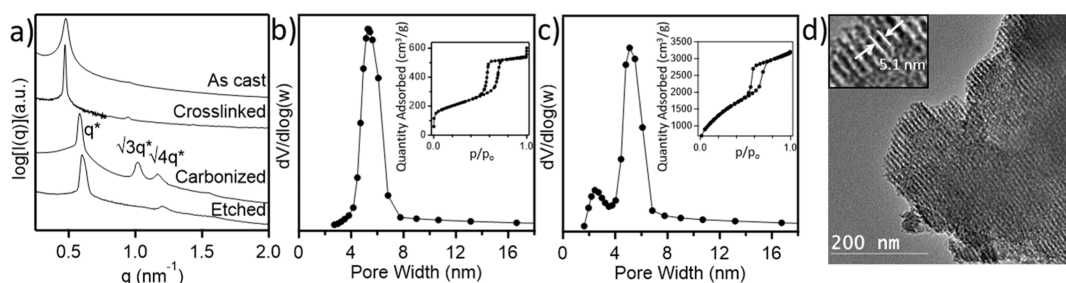


Figure 1. (a) SAXS profiles for the as-cast, crosslinked, thermally carbonized, and etched F127-templated OMC samples. Pore size distribution with an inset of the corresponding nitrogen desorption isotherm of samples after (b) carbonization and (c) etching. (d) TEM micrograph of OMC sample after etching for removal of silica.

of the plasma (around 30 W) was measured based on the area inside the charge–voltage (Q – V) Lissajous curves.⁴⁹

For plasma-assisted carbonization, 0.15 g of the crosslinked precursor was loaded into the reactor (see Figure S1 for the reactor setup). Carbonization was initiated by tuning the applied ac power to 15 kW and a frequency of 22 kHz. The carbonization reaction was operated under ambient pressure, and the reactor gas inlet was controlled by a Brooks mass flow controller at a total flow rate of 30 mL/min of Ar or an NH_3 /Ar mixture (10% and 20% of NH_3 , respectively). The carbonization was terminated immediately after the desired treatment time by turning off the AC power supply. The sample was kept under the flow of Ar until the temperature of the reactor decreased to <50 °C. For preparing control samples, the carbonization process was performed using an MTI Corporation OTF-1200 \times tube furnace under a N_2 atmosphere at the rate of 1 °C/min to 600 °C and thereafter 5 °C/min to 800 °C. After converting to carbon/silica composites, the powder was physically grinded using a mortar and pestle and then etched within a 2 M KOH solution. The solution was refreshed daily for 3 days to remove byproducts and silica. The powder was then washed several times with DI water, centrifuged to remove byproducts and residual KOH, and dried at 105 °C overnight.

2.3. Sample Characterization. A Discovery Series thermogravimetric analyzer 550 (TA Instruments) was used to determine the composition of the ordered mesoporous silica/carbon composite. Pyrolyzed samples after plasma treatment were heated to 800 °C at a rate of 20 °C/min under a nitrogen environment. The functional group composition of the prepared samples was measured on a PerkinElmer Frontier attenuated total reflection Fourier transform infrared (FTIR) spectrometer. All spectra were recorded at a wavenumber range of 4000–600 cm^{-1} with an average of 32 scans at a resolution of 4 cm^{-1} . Thermogravimetric analysis (TGA) data analysis was performed using the Trios software. X-ray photoelectron spectroscopy (XPS) was performed using a Thermo Fisher ESCALAB Xi+ spectrometer equipped with a monochromatic Al X-ray source (1486.6 eV) and a MAGCIS Ar+/Arn+ gas cluster ion sputter gun. A standard magnetic lens mode and charge compensation with a takeoff angle of 90° from the surface, a pass energy of 150 eV for survey scans with a total acquisition time of 220 s, and an energy resolution of 1.0 eV were applied. A base pressure in the analysis chamber of 3×10^{-7} mbar was set for spectral acquisition. Calibration of binding energies was conducted with respect to C 1s at 284.8 eV. Spectra were analyzed using the Thermo Fisher Advantage software.

A Micromeritics Tristar II 3020 analyzer was utilized for determining the liquid nitrogen adsorption and desorption isotherms of the mesoporous samples. Specifically, pore volumes and pore size distributions of samples were estimated from desorption isotherms at 77 K using the Barrett–Joyner–Halenda model, whereas surface areas were determined from Brunauer–Emmett–Teller analysis. The nanostructure was further characterized by small-angle X-ray scattering (SAXS) performed at the Advanced Photon Source on Beamline 12-ID-B at the Argonne National Laboratory using 14 keV X-rays. SAXS was also conducted on a Xenocs Inc. Xeuss 2.0 laboratory beamline with a sample-to-detector distance of 4.27 m using 8.05 keV X-rays. From the scattering data, the domain spacing of the OMC, d , was calculated as $d = 2\pi/q^*$, where q^* is determined by the position of the primary ordering peak in the scattering spectra. Transmission electron microscopy (TEM) images were obtained using a JEOL 2100 transmission electron microscope (accelerating voltage 200 kV) equipped with a Gatan camera.

During the carbonization process, the plasma reactor outlet was passed through a room-temperature condenser, where liquid byproducts could be collected. In order to understand the compositions of the gas-phase byproducts, a parallel experiment with a polymer precursor loading of 0.05 g was also performed. During the carbonization, the reactor outlet passing through the condenser was measured by online MS (Agilent 5973 MS equipped with MS Sensor 2.0 software, Diabolo Analytical, Inc.). To compare the compositions of the gas-phase byproducts between the thermal- and plasma-driven carbonizations, a temperature-programmed carbonization experiment was also performed with 0.05 g of the polymer precursor. Specifically, the temperature of the reactor was ramped at 5 °C/min from room temperature to 800 °C under 30 mL/min of Ar, and the reactor outlet was measured by the same online mass spectrometer. To determine the composition of the liquid byproduct, 10 μL of liquid samples collected from the condenser was diluted with 1 mL of dichloromethane. The obtained sample was analyzed on a QP2010S gas chromatograph-mass spectrometer (Shimadzu) equipped with a Rxi-5 ms (30 m, 0.25 mm ID, 0.25 μm df) column. The injection temperature was 250 °C, and the oven temperature was raised from 40 to 250 °C at a ramp of 10 °C/min.

3. RESULTS AND DISCUSSION

3.1. Comparison between Thermal and Plasma Carbonization Processes for OMC Synthesis. A model soft-templated system was first employed to understand the impact of plasma carbonization treatment on OMC morphology and pore textures. Specifically, a Pluronic surfactant

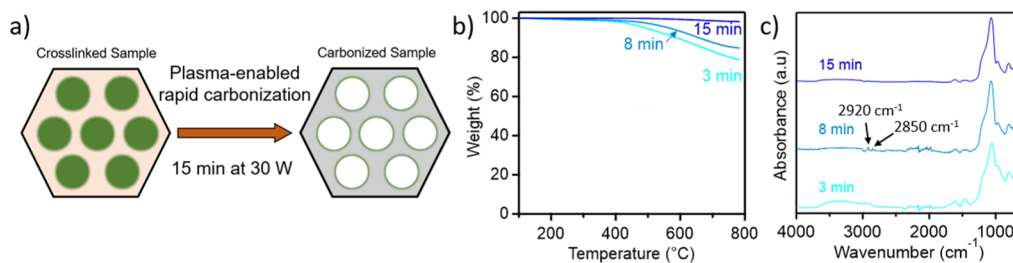


Figure 2. (a) Schematic illustration of the rapid conversion from crosslinked, micelle-templated resol-silica to OMC through plasma-treatment. (b) TGA thermograms and (c) FTIR spectra of crosslinked resol-silica following 3, 8, and 15 min of plasma treatment at 30 W.

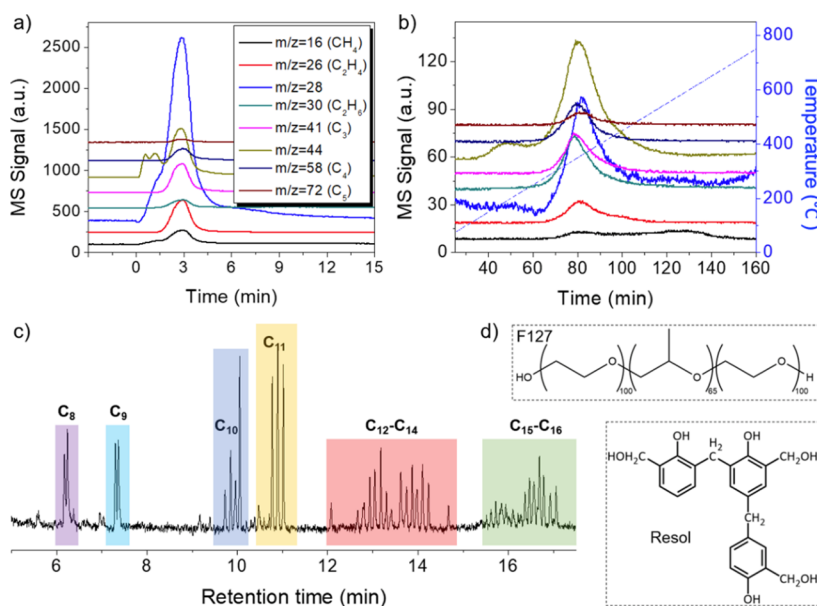


Figure 3. (a) Gas-phase signal during plasma-assisted carbonization under Ar; (b) gas-phase signal during the temperature-programmed carbonization; (c) GC–MS analysis of the liquid products collected during plasma-assisted carbonization; and (d) chemical structure of the F127 and resol.

(F127) was used to direct the assembly of TEOS and resol, forming ordered nanostructures. Upon hydrolysis and cross-linking, TEOS in the resol matrix can lead to the formation of silica.⁴⁷ After the carbonization process, OMC/silica (OMCS) composites can be obtained, and the subsequent removal of silica particles in the carbon framework can then lead to additional micropore formations. This triconstituent co-assembly approach is well-established in the field to produce OMCs with high surface areas.⁴⁷ Figure 1 demonstrates the structural characteristics of OMC control samples after each processing step, which were prepared using an electric furnace, following a conventional procedure, including 1 °C/min up to 600 °C followed by a rate of 5 °C/min to 800 °C (total heating time was 10.3 h, with an additional 6 h for cooling down to room temperature). The domain spacing of materials can be elucidated by SAXS. As shown in Figure 1a, the primary ordering peak (q^*) increased from 0.47 nm⁻¹ (as-cast) to 0.58 nm⁻¹ after carbonization, which corresponds to a domain spacing decrease from 13.3 to 10.8 nm. The one-dimensional (1D) scattering profile for the carbonized sample exhibited additional scattering peaks at $\sqrt{3}q^*$ and $\sqrt{4}q^*$, indicating the presence of a highly ordered cylindrical morphology. Following carbonization, samples were then etched in KOH solutions to remove silica nanoparticles in the carbon framework (confirmed by SEM EDAX mapping, Figures S2 and S3), which can increase the OMC surface area. Upon etching, the

domain spacing remains comparable at 10.5 nm, while the primary ordering peak remains sharp, indicating that the long-range ordered structures were retained. As illustrated in Figure 1b,c, samples after carbonization and etching steps exhibit type IV nitrogen desorption isotherms, which are consistent with OMC formation. It was found that both samples exhibit a uniform pore distribution, where the averaged pore size decreased from 5.3 to 5.1 nm in diameter upon the removal of silica. The removal of silica led to an increased surface area from 531 to 1656 m²/g, which is similar to that in a previous report.⁵⁰ The ordered structure of OMCs after the etching step was further confirmed by the TEM image in Figure 1d, where uniform pore sizes are observed in the carbon matrix with an average pore size of 5.1 nm. The pore and domain sizes of OMC from the TEM image are consistent with the results obtained from physisorption and SAXS measurements.

Figure 2a shows a brief schematic demonstration of DBD plasma-accelerated OMC synthesis. To develop an optimal plasma-assisted carbonization process for OMC synthesis, we first evaluated the necessary exposure times for a full polymer-to-carbon conversion using an initial power of 30 W (see Figure S4 for the initial electrical signals of the applied discharge). The produced carbon is electrically conductive, which would affect the stability of the plasma power. Additionally, the power will also be affected by the reactor temperature, which is rapidly increased from room temper-

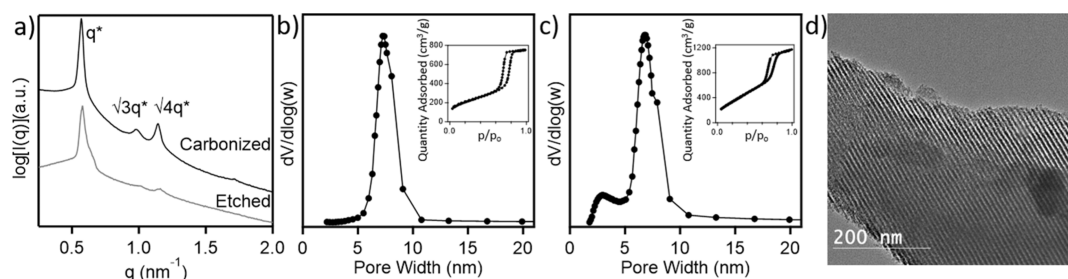


Figure 4. (a) SAXS profiles of F127-templated OMC samples after plasma-enabled carbonization and subsequent silica etching. Pore size distribution with an inset of the corresponding nitrogen desorption isotherm for (b) plasma carbonized (30 W for 15 min) and (c) etched samples. (d) TEM micrograph of corresponding OMC sample after etching.

ature to ~ 400 °C within about 10 min. From TGA measurements (under N_2 and up to 800 °C, Figure 2b), approximately 22 wt % organic residue was found in the sample after plasma treatment for 3 min, which decreased to 15 wt % after 8 min. On further extending the plasma time to 15 min, we found a near-zero mass loss (~ 0.8 wt %) in the sample, indicating that the precursors (i.e., resol) were successfully converted to carbons, and the organic template was fully decomposed. Compared to the conventional carbonization process using an electric furnace, the plasma-enabled carbonization method can reduce the processing time from at least several hours (e.g., 10.3 h for control samples in this study) to 15 min (using a 30 W source), representing more than an order of magnitude faster carbonization rate. The chemical composition of samples after different plasma times was elucidated by FTIR shown in Figure 2c. At 3 min plasma exposure, a broad intense band was observed from 2800 to 4000 cm^{-1} , corresponding to two different O–H stretching modes. This band diminishes at 8 min, where bands at 2920 and 2850 cm^{-1} can still be observed, corresponding to alkyl stretches. These bands were found to completely disappear following the complete carbonization after 15 min of plasma treatment. Since all samples contain silica particles (derived from TEOS) in the carbon framework, characteristic Si–O–Si vibrations were consistently observed, including asymmetric stretching (~ 1070 cm^{-1}) and symmetric stretching (~ 800 cm^{-1}). These results confirm that 15 min (at 30 W) is sufficient for converting crosslinked Pluronic/resol/silica blends to OMC/silica (OMCS) nanocomposites.

The gas-phase byproducts during both plasma- and thermal-assisted carbonizations were monitored by in situ mass spectrometry, and the results are shown in Figure 3a,b. Various hydrocarbons, including CH_4 , C_2H_4 , and C_2H_6 , as well as CO ($m/z = 28$) and CO_2 ($m/z = 44$), were identified. During plasma-assisted carbonization (Figure 3a), all of the gas-phase species showed peaks at approximately 3 min, indicating that the carbonization rate reached the maximum within only 3 min. The signals (except $m/z = 28$ for CO) decreased back to the baseline after 5 min, which suggested that the majority of F127 (Figure 3d) was decomposed under plasma within 5 min. Noteworthily, during plasma carbonization, the formation of aromatic compounds (benzene, toluene, and xylene) was negligible, indicating that the resol precursors were converted to OMC. In contrast, the formation of various gas-phase products during the conventional thermal carbonization process reached the peak at 360 °C and decreased back to the baseline at temperatures above 550 °C, which further confirmed the significantly slower carbonization rate using an electric furnace than using plasma. It can

be observed that the gas-phase compositions during plasma-assisted carbonization varied upon altering carbonization mechanisms, while more detailed quantification remains a challenge. In general, plasma is a quasi-neutral gas containing electrons, neutrals, electronically and vibrationally excited species, ions, radicals, and atoms. Consequently, the plasma-excited species would recombine to form new molecules other than those produced from thermal pyrolysis. For example, plasma carbonization produces more CO and C_2H_4 than thermal carbonization, which provided a possibility for simultaneously upgrading the byproducts of carbonization. Additionally, the liquid byproducts from the plasma carbonization were measured by GC–MS (see Figure 3c), from which various C_8 – C_{16} normal/iso hydrocarbons were observed.

Figure 4 shows the structural characteristics and pore textures of ordered mesoporous materials upon plasma carbonization under Ar, which were compared with control samples as shown in Figure 1. From SAXS results in Figure 4a, it was found that the domain spacing of OMC/silica composites after plasma treatment was approximately 10.7 nm, which is very similar to that of the thermally treated sample. The presence of additional scattering peaks at $\sqrt{3}q^*$ and $\sqrt{4}q^*$ indicates a high degree of ordering and cylinder-forming pore structures. After etching the silica, the domain spacing of the resulting OMC slightly changed to 10.8 nm, which is comparable to that of the thermally carbonized sample. Pore size distributions and type IV nitrogen desorption isotherms are shown in Figure 4b,c for samples after plasma treatment and etching steps, confirming the formation of OMCs. Specifically, the plasma-carbonized material exhibited a surface area of 696 m^2/g and an averaged pore size of 7.4 nm, while after etching the sample had an averaged pore size distribution of 6.9 nm and a surface area of 1346 m^2/g . Compared to the thermally carbonized sample using an electric furnace, the plasma sample exhibited a nearly identical domain spacing, an increased averaged pore size (from 5.3 to 6.9 nm), and comparable surface areas following the etching step. We attribute the large mesopore size in the plasma-carbonized samples to the rapid template removal and carbon conversion in the pyrolysis process, limiting the ability of the framework to shrink. These results confirm that the use of plasma is an effective route for OMC manufacturing while providing the great advantage of accelerated polymer-to-carbon conversion kinetics. Additionally, the mesoporous structure observed by TEM (highly ordered cylinders viewed from [110] plane, Figure 4d) is akin to the control, indicating successful carbonization through plasma treatment. A pore size of 5.5 nm is observed from the TEM image, consistent with the result

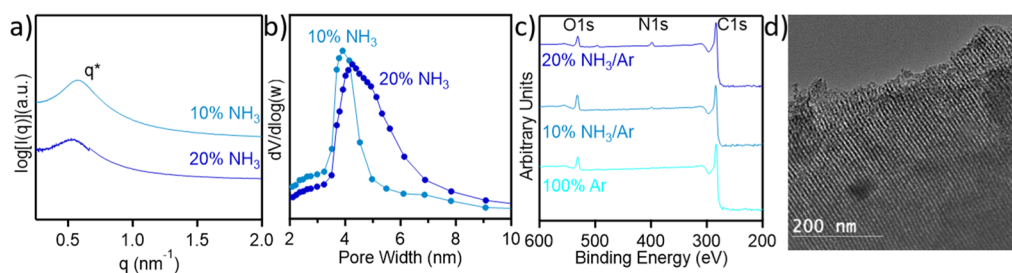


Figure 5. (a) SAXS profiles and (b) pore size distributions for etched OMC samples carbonized under 10% NH_3 /90% Ar and 20% NH_3 /80% Ar using plasma. (c) XPS of etched samples carbonized under 10% NH_3 /90% Ar, 20% NH_3 /80% Ar, and 100% Ar. (d) TEM micrograph for etched sample carbonized under 20% NH_3 /80% Ar. Samples were carbonized at 30 W for 15 min.

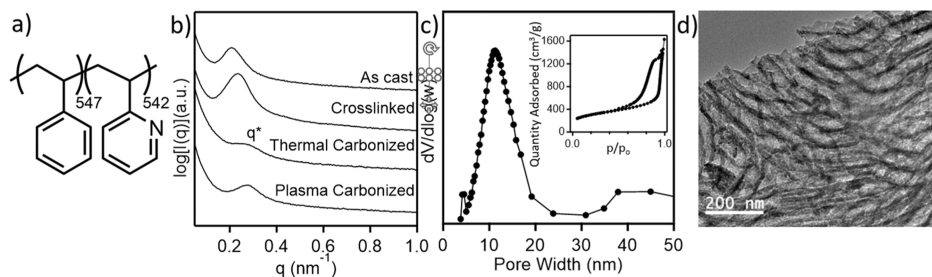


Figure 6. (a) Chemical structure of PS-*b*-P2VP block copolymer. (b) SAXS profiles for the as-cast, crosslinked, thermal carbonized, and plasma carbonized PS-*b*-P2VP-templated OMC. (c) Pore size distribution with an inset of the corresponding nitrogen desorption isotherm and (d) TEM micrograph for plasma carbonized PS-*b*-P2VP derived OMC.

obtained from physisorption measurements. These results demonstrate the capability to produce OMCs at a significantly accelerated rate through plasma-carbonization methods, which can be further extended to the functionalization of OMCs by controlling the gas atmosphere during carbonization.

3.2. OMC Doping through Plasma Treatment. The plasma carbonization strategy can be extended for incorporating heteroatoms into the OMC framework by varying the gas atmosphere. For example, the introduction of ammonia (NH_3) gas during the carbonization process can result in N-doped carbons.⁵¹ In this study, mixtures of Ar/ NH_3 gas with 10 and 20% NH_3 were employed during plasma treatment resulting in the synthesis of N-doped OMC, utilizing the same precursor composition and chemistry. As observed in Figure 5a, the ordered structures were successfully retained in the N-doped OMCs, with a domain spacing of 10.8 nm for the 10% NH_3 sample and 11.6 nm for the 20% NH_3 sample. The primary ordering peak of these doped OMC samples becomes broader than that of the undoped counterparts, suggesting that nitrogen doping during the carbonization step can reduce the degree of nanostructural ordering. Furthermore, pore size distributions of the derived OMCs are observed in Figure 5b for both samples, with an averaged pore size distribution of 3.9 and 4.3 nm for the etched samples, pyrolyzed under 10 and 20% NH_3 , respectively (sorption isotherms are included in Figures S5 and S6). It was found that the pore size of N-doped OMCs was smaller than that of undoped samples prepared under Ar, which can be attributed to swelling of the carbon framework due to nitrogen doping reactions. Similar observations were reported for samples synthesized using an electric furnace.⁵² Additionally, increasing the ammonia gas concentration from 10 to 20% resulted in a broader pore size distribution, suggesting a slight loss in the degree of ordering due to the doping reaction of the carbon framework. Moreover, the corresponding surface areas of N-doped

OMCs are 1183 and 1218 m^2/g for 10% NH_3 and 20% NH_3 samples, respectively. The presence of nitrogen within the prepared OMCs was confirmed by XPS results (Figure 5c), where nitrogen contents of 2.0 and 4.7 at % were observed for samples carbonized with the presence of 10% NH_3 and 20% NH_3 , respectively. We note that XPS is a surface technique with a typical probing depth of 5–10 nm, which can sufficiently penetrate the carbon wall (with a thickness \sim 6 nm) of these OMC samples. Furthermore, Figure 5d shows the mesoporous structure of the N-doped OMC (plasma within the mixture gas of 20% NH_3 and 80% Ar), where uniform pore sizes are found to be maintained following heteroatom incorporation with an average pore size of 4.6 nm. Thermally carbonized OMC in the presence of NH_3 has been reported to exhibit nitrogen contents between 3.6 and 6.0 at % depending on the carbonization temperature.⁵³ Moreover, Yi et al. prepared mesoporous carbon through ammoxidation before and after carbonization, with nitrogen contents of 8 at % and 1.6 at %, respectively.⁵⁴ Dai et al. also reported direct pyrolysis OMC production under NH_3 gas with nitrogen contents up to 9.3 at %.⁵⁵ Compared to these literature results, doping through plasma treatment in our system displays comparable doping levels to some of the literature reports but are lower than the observed maximum nitrogen contents. It is anticipated that increasing the NH_3 gas content during plasma carbonization may yield a higher N-doping content within the OMCs, while a careful optimization would also be required to ensure that the ordering of the nanostructure can be successfully retained. Nevertheless, the plasma-enabled functionalization and carbonization strategy is capable of producing doped OMCs at significantly elevated kinetics.

3.3. Extension to Additional OMC Systems. To further demonstrate the broad applicability of plasma-enabled carbonization, a non-Pluronic-templated, TEOS-free system was employed for OMC synthesis. After crosslinking, the precursor

material does not include the silica particles in the framework. Specifically, PS-*b*-P2VP (chemical structure shown in Figure 6a) was blended with resol oligomers, where the P2VP segment could strongly interact with hydroxyl groups from resol precursors through hydrogen bonding interactions. The total volume fraction of hydrophilic parts in the PS-*b*-P2VP/resol system was controlled to be 70%, allowing the formation of cylindrical structures. As shown in Figure 6b, the domain spacing from SAXS was found to be 29.9 nm for the as-cast, 26.5 nm after crosslinking, 22.7 nm after thermal carbonization, and 22.3 nm after plasma carbonization. The 1D SAXS scattering profile for the PS-*b*-P2VP system indicates retention of an ordered mesoporous structure throughout both thermal and plasma carbonizations, while the plasma sample exhibited an improved degree of ordering, which may be attributed to the rapid template removal that kinetically trapped the ordered structures.⁵⁶ The PS-*b*-P2VP-templated OMC exhibits type IV nitrogen desorption isotherm and pore size distribution as shown in Figure 6c, where a surface area of 955 m²/g and an averaged pore size of 11.3 nm were observed. Furthermore, the PS-*b*-P2VP-templated OMC structure was also characterized by TEM in Figure 6d, where long-range ordering and uniform pore sizes were observed with an averaged pore size of 13.8 nm. These results affirm the capability of plasma-derived OMC synthesis with non-Pluronic-templated systems. In comparison to the Pluronic-templated OMC, the domain spacing and averaged pore size of these samples are noticeably larger, which is due to the higher molecular-weight nature of PS-*b*-P2VP compared to F127. The successful synthesis of OMCs from distinct polymer/surfactant-templated systems demonstrates the broad and robust applicability of the plasma-enabled OMC fabrication method, with an accelerated rate for high-throughput material processing and discovery.

4. CONCLUSIONS

Enabling high-throughput synthesis of OMCs represents an important step for allowing an accelerated production rate at an industrial scale, as well as for efficiently navigating the material design space. Curtailing the long processing times of OMC production using conventional heating sources, this work depicts a robust strategy for accelerated OMC synthesis, utilizing DBD plasma for materials carbonization. Using a Pluronic-templated model system, the impact of processing conditions including gas atmosphere, plasma power, and time on the resulting OMC materials properties were systematically investigated; optimal conditions successfully generated functional OMCs within 15 min with a 30 W plasma source. Functionalization of OMCs during plasma carbonization was demonstrated using gas mixtures containing ammonia, resulting in a nitrogen-doping content up to 4.7 at %. This strategy can be extended to a non-Pluronic-templated system, including high-molecular-weight block copolymer/resol blends, confirming that the plasma carbonization approach is versatile and has great potential for accelerating material discovery of OMC with broad selections of template and precursor chemistries.

■ ASSOCIATED CONTENT

SI Supporting Information

The Supporting Information is available free of charge at <https://pubs.acs.org/doi/10.1021/acsomega.3c01523>.

Schematic illustration of the plasma reactor setup, SEM–EDAX analysis of OMCS and OMC, electrical signal from plasma heating, and sorption isotherms and pore size distributions of N-doped OMCs (PDF)

■ AUTHOR INFORMATION

Corresponding Authors

Yizhi Xiang – Dave C. Swalm School of Chemical Engineering, Mississippi State University, Mississippi State, Mississippi 39762, United States; orcid.org/0000-0003-4429-1754; Email: yzxiang@che.msstate.edu

Zhe Qiang – School of Polymer Science and Engineering, University of Southern Mississippi, Hattiesburg, Mississippi 39406, United States; orcid.org/0000-0002-3539-9053; Email: zhe.qiang@usm.edu

Authors

Anthony Griffin – School of Polymer Science and Engineering, University of Southern Mississippi, Hattiesburg, Mississippi 39406, United States; orcid.org/0000-0003-0526-194X

Genwei Chen – Dave C. Swalm School of Chemical Engineering, Mississippi State University, Mississippi State, Mississippi 39762, United States

Mark Robertson – School of Polymer Science and Engineering, University of Southern Mississippi, Hattiesburg, Mississippi 39406, United States

Kun Wang – Department of Physics and Astronomy and Department of Chemistry, Mississippi State University, Mississippi State, Mississippi 39762, United States; orcid.org/0000-0002-4907-310X

Complete contact information is available at:

<https://pubs.acs.org/10.1021/acsomega.3c01523>

Notes

The authors declare no competing financial interest.

■ ACKNOWLEDGMENTS

This project was partially supported by National Science Foundation under grant #OIA-1757220. This research used resources of the Advanced Photon Source, a U.S. Department of Energy (DOE) Office of Science user facility operated for the DOE Office of Science by Argonne National Laboratory under contract no. DE-AC02-06CH11357. The authors would like to acknowledge Dr. Derek Patton and Surabhi Jha for assistance with XPS experiments. This research was supported in part by a Major Research Instrumentation grant from the National Science Foundation Award (DMR-1726901). The TEM work was performed at I2AT at Mississippi State University [under support by the National Science Foundation (no. MRI-1126743)]. The authors would like to thank Dr. Xiaodan Gu and Guorong Ma for assistance with SAXS experiments.

■ REFERENCES

- (1) Ryoo, R.; Joo, S. H.; Kruk, M.; Jaroniec, M. Ordered Mesoporous Carbons. *Adv. Mater.* **2001**, *13*, 677–681.
- (2) Robertson, M.; Zagho, M. M.; Nazarenko, S.; Qiang, Z. Mesoporous Carbons from Self-Assembled Polymers. *J. Polym. Sci.* **2022**, *60*, 2015–2042.
- (3) Wu, Z.; Zhao, D. Ordered Mesoporous Materials as Adsorbents. *Chem. Commun.* **2011**, *47*, 3332–3338.
- (4) Yuan, B.; Wu, X.; Chen, Y.; Huang, J.; Luo, H.; Deng, S. Adsorption of CO₂, CH₄, and N₂ on Ordered Mesoporous Carbon:

Approach for Greenhouse Gases Capture and Biogas Upgrading. *Environ. Sci. Technol.* **2013**, *47*, 5474–5480.

(5) Saha, D.; Deng, S. Adsorption Equilibrium and Kinetics of CO₂, CH₄, N₂O, and NH₃ on Ordered Mesoporous Carbon. *J. Colloid Interface Sci.* **2010**, *345*, 402–409.

(6) Giraudet, S.; Zhu, Z.; Yao, X.; Lu, G. Ordered Mesoporous Carbons Enriched with Nitrogen: Application to Hydrogen Storage. *J. Phys. Chem. C* **2010**, *114*, 8639–8645.

(7) Xia, Y.; Mokaya, R. Ordered Mesoporous Carbon Monoliths: CVD Nanocasting and Hydrogen Storage Properties. *J. Phys. Chem. C* **2007**, *111*, 10035–10039.

(8) Liu, D.; Zheng, D.; Wang, L.; Qu, D.; Xie, Z.; Lei, J.; Guo, L.; Deng, B.; Xiao, L.; Qu, D. Enhancement of Electrochemical Hydrogen Insertion in N-Doped Highly Ordered Mesoporous Carbon. *J. Phys. Chem. C* **2014**, *118*, 2370–2374.

(9) Liu, J.; Xie, L.; Wang, Z.; Mao, S.; Gong, Y.; Wang, Y. Biomass-Derived Ordered Mesoporous Carbon Nano-Ellipsoid Encapsulated Metal Nanoparticles inside: Ideal Nanoreactors for Shape-Selective Catalysis. *Chem. Commun.* **2020**, *56*, 229–232.

(10) Perego, C.; Millini, R. Porous Materials in Catalysis: Challenges for Mesoporous Materials. *Chem. Soc. Rev.* **2013**, *42*, 3956–3976.

(11) Cao, F.; Chen, J.; Lyu, C.; Ni, M.; Gao, X.; Cen, K. Characterization and Catalytic Performances of Cu- and Mn-Containing Ordered Mesoporous Carbons for the Selective Catalytic Reduction of NO with NH₃. *Catal. Sci. Technol.* **2015**, *5*, 1267–1279.

(12) Chen, Y.; Shi, J.; Chen, Y.; Shi, L. Chemistry of Mesoporous Organosilica in Nanotechnology: Molecularly Organic–Inorganic Hybridization into Frameworks. *Adv. Mater.* **2016**, *28*, 3235–3272.

(13) Zhu, J.; Liao, L.; Bian, X.; Kong, J.; Yang, P.; Liu, B. PH-Controlled Delivery of Doxorubicin to Cancer Cells, Based on Small Mesoporous Carbon Nanospheres. *Small* **2012**, *8*, 2715–2720.

(14) Liu, C.; Yu, M.; Li, Y.; Li, J.; Wang, J.; Yu, C.; Wang, L. Synthesis of Mesoporous Carbon Nanoparticles with Large and Tunable Pore Sizes. *Nanoscale* **2015**, *7*, 11580–11590.

(15) Li, W.; Liu, J.; Zhao, D. Mesoporous Materials for Energy Conversion and Storage Devices. *Nat. Rev. Mater.* **2016**, *1*, 16023–16117.

(16) Ye, Y.; Jo, C.; Jeong, I.; Lee, J. Functional Mesoporous Materials for Energy Applications: Solar Cells, Fuel Cells, and Batteries. *Nanoscale* **2013**, *5*, 4584–4605.

(17) Linares, N.; Silvestre-Albero, A. M.; Serrano, E.; Silvestre-Albero, J.; García-Martínez, J. Mesoporous Materials for Clean Energy Technologies. *Chem. Soc. Rev.* **2014**, *43*, 7681–7717.

(18) Qiang, Z.; Liu, X.; Zou, F.; Cavicchi, K. A.; Zhu, Y.; Vogt, B. D. Bimodal Porous Carbon-Silica Nanocomposites for Li-Ion Batteries. *J. Phys. Chem. C* **2017**, *121*, 16702–16709.

(19) Zhang, R.; Du, Y.; Li, D.; Shen, D.; Yang, J.; Guo, Z.; Liu, H. K.; Elzatahry, A. A.; Zhao, D.; Zhang, R. Y.; Du, Y. J.; Shen, D. K.; Yang, J. P.; Zhao, D. Y.; Li, D.; Guo, Z. P.; Liu, H. K.; Elzatahry, A. A. Highly Reversible and Large Lithium Storage in Mesoporous Si/C Nanocomposite Anodes with Silicon Nanoparticles Embedded in a Carbon Framework. *Adv. Mater.* **2014**, *26*, 6749–6755.

(20) Liang, C.; Li, Z.; Dai, S. Mesoporous Carbon Materials: Synthesis and Modification. *Angew. Chem., Int. Ed.* **2008**, *47*, 3696–3717.

(21) Ma, T. Y.; Liu, L.; Yuan, Z. Y. Direct Synthesis of Ordered Mesoporous Carbons. *Chem. Soc. Rev.* **2013**, *42*, 3977–4003.

(22) Meng, Y.; Gu, D.; Zhang, F.; Shi, Y.; Yang, H.; Li, Z.; Yu, C.; Tu, B.; Zhao, D. Ordered Mesoporous Polymers and Homologous Carbon Frameworks: Amphiphilic Surfactant Templating and Direct Transformation. *Angew. Chem., Int. Ed.* **2005**, *44*, 7053–7059.

(23) Kopeć, M.; Lamson, M.; Yuan, R.; Tang, C.; Kruk, M.; Zhong, M.; Matyjaszewski, K.; Kowalewski, T. Polyacrylonitrile-Derived Nanostructured Carbon Materials. *Prog. Polym. Sci.* **2019**, *92*, 89–134.

(24) Ludwig, A. Discovery of New Materials Using Combinatorial Synthesis and High-Throughput Characterization of Thin-Film Materials Libraries Combined with Computational Methods. *npj Comput. Mater.* **2019**, *5*, 70–77.

(25) McFarland, E. W.; Weinberg, W. H. Combinatorial Approaches to Materials Discovery. *Trends Biotechnol.* **1999**, *17*, 107–115.

(26) Zhang, Z.; Lu, S.; Shen, G.; Zhao, Y.; Zhu, T.; Gao, Q.; Sun, N.; Wei, W. Controllable and Rapid Synthesis of Nitrogen-Doped Ordered Mesoporous Carbon Single Crystals for CO₂ Capture. *J. CO₂ Util.* **2022**, *56*, 101851.

(27) Wu, Z.; Wu, W. D.; Liu, W.; Selomulya, C.; Chen, X. D.; Zhao, D. A General “Surface-Locking” Approach toward Fast Assembly and Processing of Large-Sized, Ordered, Mesoporous Carbon Microspheres. *Angew. Chem.* **2013**, *52*, 13764–13768.

(28) Xia, Y.; Qiang, Z.; Lee, B.; Becker, M. L.; Vogt, B. D. Solid State Microwave Synthesis of Highly Crystalline Ordered Mesoporous Hausmannite Mn₃O₄ Films. *CrystEngComm* **2017**, *19*, 4294–4303.

(29) Xia, X.; Cheng, C. F.; Zhu, Y.; Vogt, B. D. Ultrafast Microwave-Assisted Synthesis of Highly Ordered Nitrogen-Doped Mesoporous Carbon. *Microporous Mesoporous Mater.* **2021**, *310*, 110639.

(30) Luong, D. X.; Bets, K. V.; Algozeeb, W. A.; Stanford, M. G.; Kittrell, C.; Chen, W.; Salvatierra, R. V.; Ren, M.; McHugh, E. A.; Advincula, P. A.; Wang, Z.; Bhatt, M.; Guo, H.; Mancevski, V.; Shahsavari, R.; Jakobson, B. I.; Tour, J. M. Gram-Scale Bottom-up Flash Graphene Synthesis. *Nature* **2020**, *577*, 647–651.

(31) Lai, L.; Li, J.; Deng, Y.; Yu, Z.; Wei, L.; Chen, Y. Carbon and Carbon/Metal Hybrid Structures Enabled by Ultrafast Heating Methods. *Small Struct.* **2022**, *3*, 2200112.

(32) Chen, W.; Li, J. T.; Wang, Z.; Algozeeb, W. A.; Luong, D. X.; Kittrell, C.; McHugh, E. A.; Advincula, P. A.; Wyss, K. M.; Beckham, J. L.; Stanford, M. G.; Jiang, B.; Tour, J. M. Ultrafast and Controllable Phase Evolution by Flash Joule Heating. *ACS Nano* **2021**, *15*, 11158–11167.

(33) Wang, L.; Seah, G. L.; Li, Y.; Tu, W. H.; Manalastas, W.; Reavley, M. J. H.; Corcoran, E. W.; Usadi, A. K.; Du, Z.; Madhavi, S.; McConnachie, J. M.; Ong, H. G.; Tan, K. W. Ultrafast Crystallization of Ordered Mesoporous Metal Oxides and Carbon from Block Copolymer Self-Assembly and Joule Heating. *Adv. Mater. Interfaces* **2022**, *9*, 2200151.

(34) Kim, S. Y.; Kim, S. Y.; Lee, S.; Jo, S.; Im, Y. H.; Lee, H. S. Microwave Plasma Carbonization for the Fabrication of Polyacrylonitrile-Based Carbon Fiber. *Polymer* **2015**, *56*, 590–595.

(35) Wei, X.; Zhang, W.; Chen, L.; Xia, X.; Meng, Y.; Liu, C.; Lin, Q.; Jiang, Y.; Gao, S. Evaluation of Graphitization and Tensile Property in Microwave Plasma Treated Carbon Fiber. *Diam. Relat. Mater.* **2022**, *126*, 109094.

(36) Zhao, W.; Lu, Y.; Wang, J.; Chen, Q.; Zhou, L.; Jiang, J.; Chen, L. Improving Crosslinking of Stabilized Polyacrylonitrile Fibers and Mechanical Properties of Carbon Fibers by Irradiating with γ -Ray. *Polym. Degrad. Stab.* **2016**, *133*, 16–26.

(37) Donnet, J. B.; Brendle, M.; Dhami, T. L.; Bahl, O. P. Plasma Treatment Effect on the Surface Energy of Carbon and Carbon Fibers. *Carbon* **1986**, *24*, 757–770.

(38) Kim, S. Y.; Kim, S. Y.; Choi, J.; Lee, S.; Jo, S. M.; Joo, J.; Lee, H. S. Two Step Microwave Plasma Carbonization Including Low Plasma Power Pre-Carbonization for Polyacrylonitrile Based Carbon Fiber. *Polymer* **2015**, *69*, 123–128.

(39) Kang, H.; Choi, S.; Lee, J. H.; Kim, K. T.; Song, Y. H.; Lee, D. H. Plasma Jet Assisted Carbonization and Activation of Coffee Ground Waste. *Environ. Int.* **2020**, *145*, 106113.

(40) Ma, X.; Li, S.; Hessel, V.; Lin, L.; Meskers, S.; Gallucci, F. Synthesis of N-Doped Carbon Dots via a Microplasma Process. *Chem. Eng. Sci.* **2020**, *220*, 115648.

(41) Wei, J.; Zhou, D.; Sun, Z.; Deng, Y.; Xia, Y.; Zhao, D. A Controllable Synthesis of Rich Nitrogen-Doped Ordered Mesoporous Carbon for CO₂ Capture and Supercapacitors. *Adv. Funct. Mater.* **2013**, *23*, 2322–2328.

(42) Qiang, Z.; Xia, Y.; Xia, X.; Vogt, B. D. Generalized Synthesis of a Family of Highly Heteroatom-Doped Ordered Mesoporous Carbons. *Chem. Mater.* **2017**, *29*, 10178–10186.

(43) Ekanayake, U. M.; Rahmati, S.; Zhou, R.; Zhou, R.; Cullen, P. J.; O’Mullane, A. P.; MacLeod, J.; Ostrikov, K. Power-to-Decarbonization: Mesoporous Carbon-MgO Nanohybrid Derived from Plasma-

Activated Seawater Salt-Loaded Biomass for Efficient CO₂ Capture. *J. CO₂ Util.* **2021**, *53*, 101711.

(44) Gao, Y.; Wang, Q.; Ji, G.; Li, A.; Niu, J. Doping Strategy, Properties and Application of Heteroatom-Doped Ordered Mesoporous Carbon. *RSC Adv.* **2021**, *11*, 5361–5383.

(45) Moosburger-Will, J.; Lachner, E.; Löffler, M.; Kunzmann, C.; Greisel, M.; Ruhland, K.; Horn, S. Adhesion of Carbon Fibers to Amine Hardened Epoxy Resin: Influence of Ammonia Plasma Functionalization of Carbon Fibers. *Appl. Surf. Sci.* **2018**, *453*, 141–152.

(46) Qiang, Z.; Guo, Y.; Liu, H.; Cheng, S. Z. D.; Cakmak, M.; Cavicchi, K. A.; Vogt, B. D. Large-Scale Roll-to-Roll Fabrication of Ordered Mesoporous Materials Using Resol-Assisted Cooperative Assembly. *ACS Appl. Mater. Interfaces* **2015**, *7*, 4306–4310.

(47) Liu, R.; Shi, Y.; Wan, Y.; Meng, Y.; Zhang, F.; Gu, D.; Chen, Z.; Tu, B.; Zhao, D. Triconstituent Co-Assembly to Ordered Mesoporous Polymer-Silica and Carbon-Silica Nanocomposites and Large-Pore Mesoporous Carbons with High Surface Areas. *J. Am. Chem. Soc.* **2006**, *128*, 11652–11662.

(48) Chen, G.; Qu, J.; Cheah, P.; Cao, D.; Zhao, Y.; Xiang, Y. Size-Dependent Activity of Iron Nanoparticles in Both Thermal and Plasma Driven Catalytic Ammonia Decomposition. *Ind. Eng. Chem. Res.* **2022**, *61*, 11436–11443.

(49) Tu, X.; Gallon, H. J.; Twigg, M. V.; Gorry, P. A.; Whitehead, J. C. Dry Reforming of Methane over a Ni/Al₂O₃ Catalyst in a Coaxial Dielectric Barrier Discharge Reactor. *J. Phys. D Appl. Phys.* **2011**, *44*, 274007.

(50) Qiang, Z.; Gurkan, B.; Ma, J.; Liu, X.; Guo, Y.; Cakmak, M.; Cavicchi, K. A.; Vogt, B. D. Roll-to-Roll Fabrication of High Surface Area Mesoporous Carbon with Process-Tunable Pore Texture for Optimization of Adsorption Capacity of Bulky Organic Dyes. *Microporous Mesoporous Mater.* **2016**, *227*, 57–64.

(51) Mahurin, S. M.; Lee, J. S.; Wang, X.; Dai, S. Ammonia-Activated Mesoporous Carbon Membranes for Gas Separations. *J. Membr. Sci.* **2011**, *368*, 41–47.

(52) Qiang, Z.; Chen, Y. M.; Xia, Y.; Liang, W.; Zhu, Y.; Vogt, B. D. Ultra-Long Cycle Life, Low-Cost Room Temperature Sodium-Sulfur Batteries Enabled by Highly Doped (N,S) Nanoporous Carbons. *Nano Energy* **2017**, *32*, 59–66.

(53) Wang, X.; Lee, J. S.; Zhu, Q.; Liu, J.; Wang, Y.; Dai, S. Ammonia-Treated Ordered Mesoporous Carbons as Catalytic Materials for Oxygen Reduction Reaction. *Chem. Mater.* **2010**, *22*, 2178–2180.

(54) Wang, X.; Liu, C. G.; Neff, D.; Fulvio, P. F.; Mayes, R. T.; Zhamu, A.; Fang, Q.; Chen, G.; Meyer, H. M.; Jang, B. Z.; Dai, S. Nitrogen-Enriched Ordered Mesoporous Carbons through Direct Pyrolysis in Ammonia with Enhanced Capacitive Performance. *J. Mater. Chem. A* **2013**, *1*, 7920–7926.

(55) Kim, N. D.; Kim, W.; Joo, J. B.; Oh, S.; Kim, P.; Kim, Y.; Yi, J. Electrochemical Capacitor Performance of N-Doped Mesoporous Carbons Prepared by Ammonia Oxidation. *J. Power Sources* **2008**, *180*, 671–675.

(56) Pagaduan, J. N.; Samitsu, S.; Varma, J.; Emrick, T.; Katsumata, R. Freeze-Burn: Fabrication of Porous Carbon Networks via Polymer-Templated Rapid Thermal Annealing. *ACS Appl. Polym. Mater.* **2022**, *4*, 4329–4338.